Gomez-Tames, Jose; Hamasaka, Atsushi; Hirata, Akimasa; Laakso, Ilkka; Lu, Mai; Ueno, Shoogo

# Group-level analysis of induced electric field in deep brain regions by different TMS coils

*Published in:*
Physics in Medicine and Biology

*DOI:*
10.1088/1361-6560/ab5e4a

Published: 16/01/2020

*Document Version*
Peer-reviewed accepted author manuscript, also known as Final accepted manuscript or Post-print

*Please cite the original version:*
Gomez-Tames, J., Hamasaka, A., Hirata, A., Laakso, I., Lu, M., & Ueno, S. (2020). Group-level analysis of induced electric field in deep brain regions by different TMS coils. *Physics in Medicine and Biology*, *65*(2), Article 025007. https://doi.org/10.1088/1361-6560/ab5e4a

# Group-Level Analysis of Induced Electric Field in Deep Brain Regions by Different TMS Coils

Jose Gomez-Tames[a], Atsushi Hamasaka[a], Akimasa Hirata[a], Ilkka Laakso[b], Mai Lu[c], and Shoogo Ueno[d],

a. Nagoya Institute of Technology, Department of Electrical and Mechanical Engineering, Nagoya, Aichi 466-8555, Japan.

b. Department of Electrical Engineering and Automation, Aalto University, FI-00076, Finland.

c. Key Lab. of Opt-Electronic Technology and Intelligent Control of Ministry of Education, Lanzhou Jiaotong University, 730070, P. R. China.

d. Department of Biomedical Engineering, Graduate School of Medicine, the University of Tokyo, Tokyo 113-0033, Japan.

*Corresponding Authors: Jose Gomez-Tames; Akimasa Hirata

Tel & Fax: +81-52-735-7916

E-mail:jgomez@nitech.ac.jp; ahirata@nitech.ac.jp

**Abstract**

Deep transcranial magnetic stimulation (dTMS) is a non-invasive technique used for the treatment of depression and obsessive compulsive disorder. In this study, we computationally evaluated group-level dosage for dTMS to characterize the targeted deep brain regions to overcome the limitations of using individualized head models to characterize coil performance in a population.

We used an inter-subject registration method adapted to the deep brain regions that enable projection of computed electric fields (EFs) from individual realistic head models ($n$ = 18) to the average space of deep brain regions. The computational results showed consistent group-level hotspots of the EF in the deep brain regions. The halo circular assembly coils induced the highest EFs in deep brain regions (up to 50% of the maximum EF in the cortex) for optimized positioning. In terms of the trade-off between field spread and penetration, the performance of the H7 coil was the best.

The computational model allowed the optimization of generalized dTMS-induced EF on deep region targets despite inter-individual differences while informing and possibly minimizing unintended stimulation of superficial regions and possible mixed stimulation effects from deep and cortical areas. These results will facilitate the decision process during dTMS interventions in clinical practice.

**Keywords:** Deep transcranial magnetic stimulation; Group-level; Electric field; Anatomical human head model; Deep brain regions

## 1. INTRODUCTION

Transcranial magnetic stimulation (TMS) (Barker, Jalinous and Freeston, 1985) is a non-invasive technique for brain neurostimulation used in clinical diagnosis and to understand brain functions in neuroscience. Recently, repetitive TMS has been used for treating different conditions such as depression or obsessive compulsive disorder (Fitzgerald, Fountain and Daskalakis, 2006; Perera *et al.*, 2016; Carmi *et al.*, 2018; Cocchi *et al.*, 2018; Pridmore *et al.*, 2018; Baeken *et al.*, 2019). During TMS, a high-intensity pulsed current is applied to a coil placed on the head, and the magnetic field generated by the coil induces eddy currents in the brain based on Faraday's law. The induced current/electric field (EF) can activate specific cortical targets.

Recent studies (Levkovitz *et al.*, 2009) indicate that deep brain regions are involved in psychoneurotic diseases such as depression. Structures related to the reward systems, including the nucleus accumbens (NAcc), ventral tegmental area, and amygdala (Nemeroff, 2002; Russo and Nestler, 2013), are located 4.5–6.5 cm from the scalp, and their stimulation can lead to antidepressant effects in deep brain stimulation (DBS) (Berton and Nestler, 2006; Schlaepfer *et al.*, 2008). Deep TMS (dTMS) has been proposed as an alternative non-invasive procedure (Levkovitz *et al.*, 2009; Tendler *et al.*, 2016; Kedzior, Gerkensmeier and Schuchinsky, 2018) and has been approved by the US Food and Drug Administration (FDA) for treatment of obsessive compulsive disorder. To stimulate the target areas located in deep regions beneath the scalp, different coils have been proposed for realizing stimulation more efficiently than with conventional figure-8 coils (Ueno, Tashiro and Harada, 1988). The proposed coils include the H-coil (Roth, Zangen and Hallett, 2002), halo figure-8 assembly (HFA) coil (Lu and Ueno, 2015), halo circular assembly (HCA) coil (Crowther *et al.*, 2011), double cone coil (Lontis, Voigt and Struijk, 2006), and H7 coil (Popa *et al.*, 2019). These new coils have been designed to overcome the trade-off between depth and dispersion (Deng, Lisanby and Peterchev, 2013; Lu and Ueno, 2017), in which reaching deeper brain structures implies a wider EF spread on the cortical and subcortical regions in the form of a potential co-activation (i.e., a possible unintended collateral stimulation) (Guadagnin *et al.*, 2016).

A previous dTMS computational study evaluated the EF strength in a sphere that mimicked the head (Deng, Lisanby and Peterchev, 2014). The findings from this study are useful for understanding the fundamental difference of the EF in deep regions. Subsequent studies evaluated the individual effects of EF in the different subcortical regions using detailed head model subjects (Fiocchi *et al.*, 2016; Guadagnin *et al.*, 2016; Lu and Ueno, 2017; Parazzini *et al.*, 2017; Samoudi *et al.*, 2018). However, EF effects derived from individualized models cannot always be generalized to a group of subjects because the EF in the brain is distorted by the brain's complicated structure, resulting in large variability (Gomez-Tames *et al.*, 2018). To overcome this

limitation, inter-subject registration methods have been applied for cortical regions to investigate group-level effects of TMS parameters and coil design in previous studies (Iwahashi *et al.*, 2017; Mikkonen *et al.*, 2018). One element that has been missing is group-level analysis in deep brain regions that is required for coil performance evaluation in dTMS.

The purpose of this study was to evaluate the induced EF in each target area of deep brain regions at a group level to characterize coil performance. Thus, we propose an inter-subject registration method for deep brain regions. This approach also permits the evaluation of the trade-off between depth and dispersion, potential co-activation, and optimization of coil location.

## 2. Method and Model

### *A. Anatomical models of the human brain*

Eighteen anatomical head models with a resolution of 0.5 mm were obtained from our previous study (Laakso *et al.*, 2015). The models were constructed from T1- and T2-weighted images acquired from a magnetic resonance image scanner (available on: http://hdl.handle.net/1926/1687). FreeSurfer image analysis software (Dale, Fischl and Sereno, 1999; Fischl, 2012) was used to reconstruct the surfaces of gray, white matter, cerebellum gray matter, cerebellum white matter, and deep brain regions (brainstem, thalamus, caudate, putamen, pallidum, hippocampus, amygdala, and NAcc). The other tissue compartments were segmented by semiautomatic methods (Laakso *et al.*, 2015, 2016) into the following: skin, fat, muscle, blood, outer skull, inner skull, intervertebral disk, ventricular cerebrospinal fluid, ventral diencephalon, mucous membrane, and dura, as shown in Fig. 1(a). Note that the cerebrospinal fluid was the volume inside the skull which was not explicitly classified as nervous tissue or blood.

### *B. Computational methods*

A volume conductor model was used to compute the induced EFs in the head models. The magneto-quasi-static approximation applies to the 10-kHz frequency band, and we assume that the displacement current is negligible when compared with the conduction current (Hirata, Ito and Laakso, 2013). In addition, the induced current does not perturb the external magnetic field. The induced scalar potential $\varphi$ is given by

$$\nabla\left[\sigma\left(\nabla\varphi+\frac{\partial \boldsymbol{A_0}}{\partial t}\right)\right]=\mathbf{0} \qquad (1)$$

where $\boldsymbol{A}_0$ and $\sigma$ denote the magnetic vector potential of the applied magnetic field and tissue conductivity, respectively. The induced EF was calculated from the gradient of the scalar potential by the following expression:

$$\mathbf{E} = -\boldsymbol{\nabla}\varphi - \frac{\partial A_0}{\partial t}. \qquad (2)$$

Eq. (1) can be numerically solved using the finite-element method (FEM) with first-order 0.5 mm × 0.5 mm × 0.5 mm cubic elements (Laakso and Hirata, 2012). The electric conductivity of the head tissues was assumed to be linear and isotropic. As shown in Table 1, a different tissue conductivity was assigned to each tissue based on the fourth-order Cole-Cole model at 10 kHz (Gabriel, Lau and Gabriel, 1996). The coil current was fixed to 1 A for all simulations. Associated numerical errors were marginal considering the model resolution (Gomez-Tames *et al.*, 2017; Gomez-Tames, Tarnaud, *et al.*, 2019) and experimental verifications (Laakso *et al.*, 2017; Aonuma *et al.*, 2018; Mikkonen *et al.*, 2018). In addition, averaging over multiple subjects further reduced the error in the mean EF strength, as described in the next subsection.

### *C. Registration method*

Surface data in the seven deep brain structures (brainstem, caudate, putamen, hippocampus, amygdala, NAcc, and thalamus) were registered to the deep regions of the MNI ICBM 2009a standard template (Fonov *et al.*, 2009, 2011). For each deep brain region, we took the surface mesh and the same surface for the MNI template and used an iterative closest point method (part of the Visualization Toolkit (VTK)) to obtain an affine registration between the surfaces. For each point $y$ in the template surface of a deep region $Y$, we found the closest point $x$ in the registered individual deep region $X$ via the minimum Euclidian distance ($f: Y \to X$). If $E$ was the EF magnitude from an individual deep region, the template EF at y was calculated by $E\big(f(y)\big)$ (Gomez-Tames, Asai, *et al.*, 2019). The process was repeated for each deep region and summarized in Fig. 1(c). In addition to deep brain regions, the surface EFs were registered to the surface of the brain of the MNI ICBM 2009a standard template using a previously described registration procedure for potential co-activation analysis, as shown in Fig. 5(b) (Laakso *et al.*, 2015).

### *D. Group-level EF characterization*

To compare the characteristics of dTMS coils, the group-level EF was used, which was the average of the registered EF strengths (absolute value) in the standard brain space between all subjects for the seven deep brain regions to minimize inter-individual effects. The inter-individual effect was quantified by the relative standard deviation of the EFs. In addition, the EFs were normalized with the maximum value in the cerebral cortex to facilitate comparison between coils despite differences in coil design and number of turns. To mitigate the numerical artifacts derived from computing the EF with the voxel model at the surface of the CSF–brain boundaries (Reilly and Hirata, 2016), the top 0.1% of the gray-matter EFs, sorted in ascending order, were removed as post-processing artifacts (99.9$^{\text{th}}$ percentile value of the EF). The magnitude of the

discarded fields is up to 1.4 times the 99.9$^{th}$ value. (Gomez-Tames et al., 2017).

Some points on the individual surface were possibly not assigned to the standard deep brain template with the potential loss of hotspots or EF information because of the minimum Euclidian distance criteria. We defined a metric of the registration error to investigate the potential information loss. The registration error for each subject was the difference between two EF distributions: (i) $E(x)$ which is the original EF in the individual deep regions and (ii) $E\left(f\left(g(x)\right)\right)$ which is the registration of $E\left(f(y)\right)$ back to the individual deep region and is given using the Euclidean distance ($g: X \rightarrow Y$) as follows

$$\text{Registration Error} = \left|E(x) - E\left(f\left(g(x)\right)\right)\right|. \qquad (3)$$

In this study, we adopted the EF strength to describe regions with a high possibility of stimulation. The rationale is that even in the cerebral cortex, where there is a highly uniform orientation of the pyramidal neurons relative to the cortical surface, a consensus of the most appropriate EF direction has not been established (Fox *et al.*, 2004; Bungert *et al.*, 2016; Laakso *et al.*, 2017). In the case of the deep brain regions, the orientation of most neurons, which is important to determine the most effective EF direction, is not clear except for the hippocampus.

### *E. Coil positioning scenarios and modeling*

Group-level EF comparisons of seven coils were conducted for the two scenarios. In the first scenario (subsection 3.A to 3.C), all coils were centered at the same position (Cz or AFz) in all subjects to reduce intra-subject anatomical variations of the tissues underneath the coil (e.g., the distance to deep regions), except the H1 coil that was placed on the frontal region (around AFz) and adjusted to fit head geometry. In the second scenario (subsection 3.D), coils were compared using optimized coil locations based on the 10-10 international EEG system. Locations were omitted if the windings crossed the head model. All coils were optimized using a medial–lateral coil orientation.

A schematic representation of the seven coils is shown in Fig. 2. Fig. 2(a) shows a circular coil whose inner and outer radii are 35 and 45 mm, respectively. The number of turns is 14. Fig. 2(b) shows a commonly used figure-8 coil whose inner and outer radii are 23.5 and 48.5 mm, respectively. The number of turns is nine. Fig. 2(c) shows the H-coil based on a previous study (Lu and Ueno, 2017). The coil has 13 windings and consists of base and return parts. The base part is oriented along the anterior-posterior axis on the left hemisphere, thus stimulating neuronal pathways along this axis. The return part directs the return currents on the right hemisphere. Fig. 2(d) shows an HCA coil, which combines the circular and halo coils. The halo coil

radii are 138 and 144 mm, and their position is 100 mm below the figure-8 coil. The number of turns is five. Fig. 2(e) shows the figure-8 assembly coil, which combines the figure-8 and halo coils. Fig. 2(f) shows the double cone coil, in which the angle formed between the two circular coils is 95° (instead of 180°), as with the figure-8 coil. The inner and outer radii of the circular coils are 48 and 65 mm, respectively, and the number of turns is nine. Fig. 2(g) shows the H7 coil, consisting of two adjacent wings fixed at a relative angle of 90°. Each wing consists of two layers of concentric elliptical windings with the major axis ranging from 75–140 mm, and the minor axis ranging from 70−125 mm; and the number of turns is four.

### *F. EF penetration and spread*

The penetration depth and spread of the EF from the cortex were examined. Specifically, the spread to the "depth" direction was quantified by examining the penetration and volume of the EF. The "depth" direction was defined using a method described previously (Guadagnin *et al.*, 2016). In brief, the "center" of the brain was defined under Cz at a height of T3 and T4 by the 10-20 EEG system. In addition, we determined the locations ("cortical spots") where fields are larger than $0.95\times EF_{max}$ on the cortex. Note that the position of the original maximum value and 99.9$^{th}$ percentile value was nearly the same. The direction that yielded the deepest value from the "cortical spots" to the "center" was defined as the "depth" direction, as shown in Fig. 1(b). Moreover, the half-value spread metric (inverse of focality) was used to indicate the spread in the "depth" direction as follows:

$$S_{1/2} = \frac{V_{1/2}}{d_{1/2}} \qquad (4)$$

where $V_{1/2}$ is the half-value volume defined as the volume in the brain region in which the EF is equal to or greater than 50% of the value of EF on the "cortical spot". The term $d_{1/2}$ is the half-value depth corresponding to the maximum depth in which the EF is equal to or greater than 50% of the EF value on the "cortical spot". We calculated the mean value and standard deviation of $d_{1/2}$, $V_{1/2}$, and $S_{1/2}$ for 18 models.

## 3. COMPUTATIONAL RESULTS

### *A. EF registration*

Fig. 3(a) illustrates the effect of individual variability on EF distribution of the seven deep brain regions for the case of the HCA coil. For instance, we can observe a distinct EF pattern in the amygdala for subject 10 and subject 11. To investigate group-level EF effects, the individual deep EFs are transformed to the standard deep brain template EFs because of the high-interindividual anatomical difference, as shown in Fig. 3(b). Visual inspection shows an adequate matching between individual and template EF distributions. In addition, Fig. 3(c) confirms good matching with a median registration error of 2.6 mV/m (individual deep

regions range: 1.3-4.2 mV/m) or normalized median error of 0.7%.

*B. Group-level EF distribution difference between coils*

Fig. 4(a) shows the group-averaged ($n$ = 18) EF distribution in the standard space of the seven deep brain regions for all coils centered at the same position (except H1 in the frontal region) to exclude intra-subject differences (i.e., distance to deep regions). The HFA and HCA coils induced the highest EFs in the deep regions with respect to cortical EFs. In contrast, circular and figure-8 coils produced weaker EFs. High EFs were distributed mostly in the caudate and putamen for all coils. The third structure with higher EFs was variable among the coils (e.g., hippocampus for HFA and HCA coils and brainstem for figure-8 coil). In addition, Fig. 4(b) shows the standard deviation of the induced EF for each coil. The caudate region presents a larger variation for this configuration.

*C. Trade-off between depth, spread, and potential co-activation.*

Fig. 5(a) shows the trade-off relationship between $S_{1/2}$ and $d_{1/2}$ considering field values normalized by the maximum cortical EF. The ideal coil for dTMS would generate a high induced EF in deep regions (high $d_{1/2}$) with a small spread (small $S_{1/2}$). An intercomparison was conducted for coils to analyze the trade-off for coils centered at Cz or AFz locations (H1 only in AFz). The penetration depths using the half-value metric correspond to the subcortical regions (<3.5 cm from the cortical surface). The HCA coil produced the highest penetration but with a higher spread. In general, H7 coil had a good trade-off between depth and spread, although the trade-off could change with the same coil at different regions because of coil geometry (i.e., how the shape and casing conform to the head and relative position to the targets).

Potential co-activation of superficial brain regions is a consequence of the trade-off between depth and spread. A group-level map ($n$ = 18) of the cortical and subcortical EFs is presented to quantify the effects of potential co-activation in Fig. 5(b). From the coils with higher EF percentage in deep brain regions (i.e., HCA and HFA coils), potential co-activation of the HCA coil was mainly in the prefrontal and occipital areas, whereas the HFA coil exhibited a large potential co-activation in the cortical and subcortical regions below the Cz position. The double cone coil exhibited higher penetration than the figure-8 coil but also led to considerable potential co-activation. In addition, H1 was found to be more suitable for focal activation of the prefrontal cortex and underlying subcortical regions. H7 could activate deeper regions but with higher potential co-activation than H1.

*D. Optimized group-level EF distribution*

The coil position was optimized to maximize the group-level EF in different deep brain regions, as shown in Fig. 6(a). The coils were centered on scalp positions according to 10-10 EEG international system in all subjects. The results showed that the HCA coil had the highest group-level EF (up to 50% in most of the

deep brain regions), while the double cone coil exhibited the smallest group-level EF (up to 30% in deep brain regions). Figure-8 also presents high EFs in the hippocampus and amygdala relative to cortical EF; however, the dTMS-induced EF is limited by the TMS device power for the figure-8 coil (Table A1, Appendix A). In contrast, the double cone or H7 coils can penetrate deeper with higher EF at the expense of induced higher and wider spread electrical fields in superficial cortical regions. The optimal location of the figure-8 coil is the temporal region, whereas the optimal locations for double cone and H7 coils was along the midline.

In the case of the HCA coil, the optimal location is around FC3 for caudate, putamen, and NAcc, and around CP3 for the other deep regions. We also investigated the optimal coil location for all deep brain regions by averaging the normalized EF scalp maps across all deep regions for the same coil. We found that the HFA coil (AFz or CPz), double cone (AFz), and H7 (F1) coils are optimal at the medial scalp positions. In contrast, HCA (CP3), circular (FC5), and figure-8 (FT9) coils are optimal at more lateral scalp locations, as shown in Fig. 6(b).

## 4. DISCUSSION

We proposed a group-level EF approach in deep regions that allows generalizing the coil performance for dTMS in a group of subjects to overcome the limitation of using individualized head models to characterize coil performance in a population (Lu and Ueno, 2017). For instance, Fig. 3(a) shows the variation in EF distribution in deep regions of 18 subjects for the same coil according to subject anatomical differences in the head tissues. This agrees with previous studies where significant differences in the EF cortical distribution were observed in regions with higher individual neuroanatomical differences (Gomez-Tames *et al.*, 2018). A reliable registration method was implemented to obtain group-level EF distributions in the standard space of deep brain regions to minimize subject differences (Fig. 3).

### *A. dTMS coil characterization by group-level EF*

The dTMS coils were characterized by investigating the group-level EF distribution, trade-off between spread and depth, and potential co-activation. For fair characterization of the coil design, the coils were centered at the same location to reduce intra-subject differences (e.g., distance to the deep regions if coils are placed at different locations in the same subject).

First, we observed consistent group-level EF hotspots on surfaces of the deep brain regions, which suggested the possibility of targeting specific deep brain regions in Fig. 4(a). The HFA and HCA coils induced the highest EF in all deep brain regions. The effect of the Halo coil on these configurations permits high values because of the high-penetration depth but with higher spread (Lu and Ueno, 2015). We also

confirmed that the EF distribution of the HFA coil was asymmetric as the magnetic field was strengthened on one side because this was the same direction of the current in the halo coil and one circular coil of the figure-8 coil. By contrast, the magnetic field on the other side was weakened because of the opposite effect.

Second, the most appropriate choice of coil settings should also be based on a well-balanced evaluation of penetration depth and focality. Fig. 5A confirmed that the relationship between the penetration depth and spread was a trade-off. The coil ranking and depth values according to the half-depth metric agrees with the results of a previous study (Deng, Lisanby and Peterchev, 2013), although larger half-depth values have been reported in other studies (Guadagnin *et al.*, 2016; Parazzini *et al.*, 2017). The maximum penetration was smaller than 4 cm from the cortical surface; however, the group-average distance from the closest points between the scalp and each deep brain structure was approximately 4.3 to 6.6 cm, as shown in Table 2. Thus, the half-value metric is useful for evaluating EFs in subcortical regions but is not suitable for EFs in deep brain regions. For the case of subcortical regions, the H7 coil exhibits a good trade-off between depth and spread.

Third, the concerns/implications of potential co-activation can be categorized into two groups: clinical side-effects and mixed stimulation effects. Clinical side-effects include transient headache or discomfort at the site of stimulation and seizure, and the latter is a major adverse event. A recent study showed that the risk ratio (seizures per exposure) for H-coil (0.43/1000) was higher than double cone (0.12/1000) and figure-8 coils (0.08/1000), although the number of H-coil or double cone sessions in the sample was small (Lerner, Wassermann and Tamir, 2019). Mixed stimulation effects refer to unintended collateral stimulation of cortical and subcortical circuits with associated circuits to deep brain regions. Consequently, the assumption that dTMS is acting only on specific deep brain regions should be taken with care. In addition, the assumption that the stimulation of superficial regions is acceptable or whether activation of superficial regions has no indirect effect on deep regions needs to be further analyzed. We showed that computational model approaches are helpful in optimizing dTMS to maximize dosage in deep brain regions while informing and possibly minimizing potential unintended stimulation.

### *B. Optimized dTMS localization by group-level EF*

To determine the maximum group-level EFs, scalp maps of EFs showed the best locations in each deep region or whole deep regions for a population, as shown in Figs. 6(a) and 6(c), respectively. This method can be used to characterize and optimize dTMS coils in clinical applications where the same location is used in all subjects (one-for-all approach) usually based on the 10-10 EEG international system. Optimized coil location induced a maximum group-level EF of 30-50% of the maximum EF value of the brain surface or 15-25% of the scalp surface. As a reference, this percentage was smaller than the one observed in transcranial direct current stimulation (70% of the maximum EF value on the brain surface) (Gomez-Tames, Asai and

Hirata, 2019). The HCA coil induced the larger EF, and the figure-8 coil also presented high EFs (45%) in the hippocampus and amygdala for stimulation optimized for temporal location. One disadvantage of stimulation in the temporal region is that the pain perception threshold can be smaller than that in the parietal region. Even though optimized locations were explored, the EF levels (<50%) indicate that it is unlikely that dTMS can stimulate these deep areas without considerable side-effects caused by the much stronger potential co-activation of other regions. In addition to the normalized EFs relative to the maximum on the cortex, we investigated the percentage of the maximum stimulation output (MSO) required to achieve similar EF levels in deep regions, as shown in Table A1 of Appendix A. The maximum MSO can be exceeded for some coils to target specific deep brain regions. The HFA and HCA coils may require lower stimulation intensity to achieve a similar EF in deep brain regions. Finally, this study used the medial–lateral coil orientation for optimization of the coil location because optimization based on coil orientation would lead to negligible improvement in the dTMS-induced EFs for the medial–lateral direction, as shown in Appendix B.

## 5. Conclusion

This study revealed the variability in EF distributions in deep brain regions resulting from inter-individual differences during dTMS. Despite these inter-individual variations, the proposed registration method for deep regions could help determine a systematic tendency of the EF to derive the optimal coil for a group of subjects but with levels below 50% in comparison to cortical EFs for optimized coil localization. As a result, the first generalized map of targeted areas by different coils was presented for dTMS. These maps will enable the delivery of the most optimal dosage to the desired target while also accounting for potential collateral stimulation as an important factor to be included in dTMS studies. Future studies can use this approach to investigate new coil designs to facilitate maximum EF on specific deep structures and analyze the effects on different population segments (e.g., gender and age).

## Appendix A: Maximum Stimulation Output Requirements

To induce the same level of EF in the deep brain regions, each coil may require a different percentage of the maximum stimulation output (MSO). A coil current intensity of 174 A/μs was used for 100% MSO, similar to Magstim 200 stimulator (Laakso *et al.*, 2017). Table A1 shows that the % MSO is exceeded for circular, figure-8, and H coils when targeting specific deep brain regions for an induced EF strength of 50 V/m (Casali *et al.*, 2010). The other coils are more suitable for achieving a larger field strength within the output capability of the TMS device.

## APPENDIX B: OPTIMIZED COIL ORIENTATION

The dTMS-induced EF variation due to coil orientation was investigated for the HFA and figure-8 coils. Coil optimization for circular and HCA coils are not considered due to coil symmetry. In addition, medial–lateral orientation was found to be optimal for the double cone and H7 coils to fit the head shape. The coil was rotated from 0° (medial–lateral orientation) to 150° with steps of 30° in an anticlockwise direction (superior view of coil). The coil was located in the same scalp positions, as shown in Fig. 6A. The improvement in the EF on different regions was quantified by the percentage point variation, taking the EF for the medial–lateral orientation as reference. Figure A1 shows no significant variation of the EF owing to coil orientation variation at the optimized coil position for deep brain regions (negligible for the HFA coil and less than 6% percentage points for the figure-8 coil at 120°).

## ACKNOWLEDGMENT

This work was supported by a Grant-in-Aid for Scientific Research (A) (JSPS KAKENHI 17H05293) and a Grant-in-Aid for Early-Career Scientists (JSPS KAKENHI 19K20668) from the Japanese Society for the Promotion of Science (JSPS).

## REFERENCES


Aonuma, S., Gomez-Tames, J., Laakso, I., Hirata, A., Takakura, T., Tamura, M. and Muragaki, Y. (2018) 'A high-resolution computational localization method for transcranial magnetic stimulation mapping', *NeuroImage*, 172, pp. 85–93. doi: 10.1016/j.neuroimage.2018.01.039.

Baeken, C., Brem, A.-K., Arns, M., Brunoni, A. R., Filipčić, I., Ganho-Ávila, A., Langguth, B., Padberg, F., Poulet, E., Rachid, F., Sack, A. T., Vanderhasselt, M.-A. and Bennabi, D. (2019) 'Repetitive transcranial magnetic stimulation treatment for depressive disorders: current knowledge and future directions.', *Current opinion in psychiatry*, 32(5), pp. 409–415. doi: 10.1097/YCO.0000000000000533.

Barker, A. T., Jalinous, R. and Freeston, I. L. (1985) 'Non-invasive magnetic stimulation of human motor cortex', *Lancet (London, England)*, 1(8437), pp. 1106–7.

Berton, O. and Nestler, E. J. (2006) 'New approaches to antidepressant drug discovery: beyond monoamines', *Nature Reviews Neuroscience*, 7(2), pp. 137–151. doi: 10.1038/nrn1846.

Bungert, A., Antunes, A., Espenhahn, S. and Thielscher, A. (2016) 'Where does TMS Stimulate the Motor Cortex? Combining Electrophysiological Measurements and Realistic Field Estimates to Reveal the Affected Cortex Position', *Cerebral Cortex*, 120, pp. 141–157. doi: 10.1093/cercor/bhw292.

Carmi, L., Alyagon, U., Barnea-Ygael, N., Zohar, J., Dar, R. and Zangen, A. (2018) 'Clinical and electrophysiological outcomes of deep TMS over the medial prefrontal and anterior cingulate cortices in OCD patients', *Brain Stimulation*. Elsevier Inc., 11(1), pp. 158–165. doi: 10.1016/j.brs.2017.09.004.

Casali, A. G., Casarotto, S., Rosanova, M., Mariotti, M. and Massimini, M. (2010) 'General indices to characterize the electrical response of the cerebral cortex to TMS', *NeuroImage*, 49(2), pp. 1459–1468. doi: 10.1016/j.neuroimage.2009.09.026.

Cocchi, L., Zalesky, A., Nott, Z., Whybird, G., Fitzgerald, P. B. and Breakspear, M. (2018) 'Transcranial magnetic stimulation in obsessive-compulsive disorder: A focus on network mechanisms and state dependence', *NeuroImage: Clinical*. Elsevier Inc., pp. 661–674. doi: 10.1016/j.nicl.2018.05.029.

Crowther, L. J., Marketos, P., Williams, P. I., Melikhov, Y., Jiles, D. C. and Starzewski, J. H. (2011) 'Transcranial magnetic stimulation: Improved coil design for deep brain investigation', *Journal of Applied Physics*. American Institute of Physics, 109(7), p. 07B314. doi: 10.1063/1.3563076.

Dale, A. M., Fischl, B. and Sereno, M. I. (1999) 'Cortical Surface-Based Analysis', *NeuroImage*, 9(2), pp. 179–194. doi: 10.1006/nimg.1998.0395.

Deng, Z.-D., Lisanby, S. H. and Peterchev, A. V. (2013) 'Electric field depth–focality tradeoff in transcranial magnetic stimulation: Simulation comparison of 50 coil designs', *Brain Stimulation*, 6(1), pp. 1–13. doi: 10.1016/j.brs.2012.02.005.

Deng, Z.-D., Lisanby, S. H. and Peterchev, A. V. (2014) 'Coil design considerations for deep transcranial magnetic stimulation', *Clinical Neurophysiology*. Elsevier, 125(6), pp. 1202–1212. doi: 10.1016/J.CLINPH.2013.11.038.

Fiocchi, S., Longhi, M., Ravazzani, P., Roth, Y., Zangen, A. and Parazzini, M. (2016) 'Modelling of the Electric Field Distribution in Deep Transcranial Magnetic Stimulation in the Adolescence, in the Adulthood, and in the Old Age', *Computational and Mathematical Methods in Medicine*. Hindawi Publishing Corporation, 2016, pp. 1–9. doi: 10.1155/2016/9039613.

Fischl, B. (2012) 'FreeSurfer', *NeuroImage*, 62(2), pp. 774–781. doi: 10.1016/j.neuroimage.2012.01.021.

Fitzgerald, P., Fountain, S. and Daskalakis, Z. (2006) 'A comprehensive review of the effects of rTMS on motor cortical excitability and inhibition', *Clinical Neurophysiology*, 117(12), pp. 2584–2596. doi: 10.1016/j.clinph.2006.06.712.

Fonov, V., Evans, A. C., Botteron, K., Almli, C. R., McKinstry, R. C., Collins, D. L. and Brain Development Cooperative Group (2011) 'Unbiased average age-appropriate atlases for pediatric studies', *NeuroImage*. NIH Public Access, 54(1), pp. 313–27. doi: 10.1016/j.neuroimage.2010.07.033.

Fonov, V., Evans, A., McKinstry, R. and Almli, C. (2009) 'Unbiased nonlinear average age-appropriate brain templates from birth to adulthood', *Neuroimage*, 47, p. S102. doi: https://doi.org/10.1016/S1053-8119(09)70884-5.

Fox, P. T., Narayana, S., Tandon, N., Sandoval, H., Fox, S. P., Kochunov, P. and Lancaster, J. L. (2004) 'Column-based model of electric field excitation of cerebral cortex', *Human Brain Mapping*, 22(1), pp. 1–14. doi: 10.1002/hbm.20006.

Gabriel, S., Lau, R. W. and Gabriel, C. (1996) 'The dielectric properties of biological tissues: III. Parametric models for the dielectric spectrum of tissues', *Physics in medicine and biology*. IOP Publishing, 41(11), p. 2271. doi: 10.1088/0031-9155/41/11/003.

Gomez-Tames, J., Asai, A. and Hirata, A. (2019) 'Significant Group-Level Hotspots Found in Deep Brain Regions during tDCS: A Computational Analysis of Electric Field', *Clinical Neurophysiology*.

Gomez-Tames, J., Asai, A., Mikkonen, M., Laakso, I., Tanaka, S., Uehara, S., Otaka, Y. and Hirata, A. (2019) 'Group-level and functional-region analysis of electric-field shape during cerebellar transcranial

direct current stimulation with different electrode montages', *Journal of Neural Engineering*. IOP Publishing, 16(3), p. 36001. doi: 10.1088/1741-2552/ab0ac5.

Gomez-Tames, J., Hamasaka, A., Laakso, I., Hirata, A. and Ugawa, Y. (2018) 'Atlas of optimal coil orientation and position for TMS: A computational study', *Brain Stimulation*. Elsevier, 11(4), pp. 839–848. doi: 10.1016/j.brs.2018.04.011.

Gomez-Tames, J., Laakso, I., Haba, Y., Hirata, A., Poljak, D. and Yamazaki, K. (2017) 'Computational Artifacts of the In Situ Electric Field in Anatomical Models Exposed to Low-Frequency Magnetic Field', *IEEE Transactions on Electromagnetic Compatibility*, 60(3), pp. 589–597. doi: 10.1109/TEMC.2017.2748219.

Gomez-Tames, J., Tarnaud, T., Miwa, K., Hirata, A., Van de Steene, T., Martens, L., Tanghe, E. and Joseph, W. (2019) 'Brain Cortical Stimulation Thresholds to Different Magnetic Field Sources Exposures at Intermediate Frequencies', *IEEE Transactions on Electromagnetic Compatibility*, pp. 1–9. doi: 10.1109/TEMC.2019.2943138.

Guadagnin, V., Parazzini, M., Fiocchi, S., Liorni, I. and Ravazzani, P. (2016) 'Deep Transcranial Magnetic Stimulation: Modeling of Different Coil Configurations', *IEEE Transactions on Biomedical Engineering*, 63(7), pp. 1543–1550. doi: 10.1109/TBME.2015.2498646.

Hirata, A., Ito, F. and Laakso, I. (2013) 'Confirmation of quasi-static approximation in SAR evaluation for a wireless power transfer system', *Physics in Medicine and Biology*, 58(17), pp. N241–N249. doi: 10.1088/0031-9155/58/17/N241.

Iwahashi, M., Gomez-Tames, J., Laakso, I. and Hirata, A. (2017) 'Evaluation method for *in situ* electric field in standardized human brain for different transcranial magnetic stimulation coils', *Physics in Medicine and Biology*. IOP Publishing, 62(6), pp. 2224–2238. doi: 10.1088/1361-6560/aa5b70.

Kedzior, K. K., Gerkensmeier, I. and Schuchinsky, M. (2018) 'Can deep transcranial magnetic stimulation (DTMS) be used to treat substance use disorders (SUD)? A systematic review.', *BMC psychiatry*, 18(1), p. 137. doi: 10.1186/s12888-018-1704-0.

Laakso, I. and Hirata, A. (2012) 'Fast multigrid-based computation of the induced electric field for transcranial magnetic stimulation', *Physics in medicine and biology*, 57(23), pp. 7753–7765.

Laakso, I., Murakami, T., Hirata, A. and Ugawa, Y. (2017) 'Where and what TMS activates: Experiments and modeling', *Brain Stimulation*. Elsevier. doi: 10.1016/J.BRS.2017.09.011.

Laakso, I., Tanaka, S., Koyama, S., De Santis, V. and Hirata, A. (2015) 'Inter-subject variability in electric

fields of motor cortical tDCS', *Brain Stimulation*, 8(5), pp. 906–913. doi: 10.1016/j.brs.2015.05.002.

Laakso, I., Tanaka, S., Mikkonen, M., Koyama, S., Sadato, N. and Hirata, A. (2016) 'Electric fields of motor and frontal tDCS in a standard brain space: A computer simulation study', *NeuroImage*, 137, pp. 140–151. doi: 10.1016/j.neuroimage.2016.05.032.

Lerner, A. J., Wassermann, E. M. and Tamir, D. I. (2019) 'Seizures from transcranial magnetic stimulation 2012–2016: Results of a survey of active laboratories and clinics', *Clinical Neurophysiology*. Elsevier Ireland Ltd, 130(8), pp. 1409–1416. doi: 10.1016/j.clinph.2019.03.016.

Levkovitz, Y., Harel, E. V., Roth, Y., Braw, Y., Most, D., Katz, L. N., Sheer, A., Gersner, R. and Zangen, A. (2009) 'Deep transcranial magnetic stimulation over the prefrontal cortex: Evaluation of antidepressant and cognitive effects in depressive patients', *Brain Stimulation*, 2(4), pp. 188–200. doi: 10.1016/j.brs.2009.08.002.

Lontis, E. R., Voigt, M. and Struijk, J. J. (2006) 'Focality Assessment in Transcranial Magnetic Stimulation With Double and Cone Coils', *Journal of Clinical Neurophysiology*, 23(5), pp. 463–472. doi: 10.1097/01.wnp.0000229944.63011.a1.

Lu, M. and Ueno, S. (2015) 'Deep Transcranial Magnetic Stimulation Using Figure-of-Eight and Halo Coils', *IEEE Transactions on Magnetics*, 51(11), pp. 1–4. doi: 10.1109/TMAG.2015.2436977.

Lu, M. and Ueno, S. (2017) 'Comparison of the induced fields using different coil configurations during deep transcranial magnetic stimulation', *PLOS ONE*. Edited by T. Yuan. Public Library of Science, 12(6), p. e0178422. doi: 10.1371/journal.pone.0178422.

Mikkonen, M., Laakso, I., Sumiya, M., Koyama, S., Hirata, A. and Tanaka, S. (2018) 'TMS motor thresholds correlate with TDCS electric field strengths in hand motor area', *Frontiers in Neuroscience*. Frontiers, 12, p. 426. doi: 10.3389/fnins.2018.00426.

Nemeroff, C. B. (2002) 'Recent advances in the neurobiology of depression.', *Psychopharmacology bulletin*, 36 Suppl 2, pp. 6–23.

Parazzini, M., Fiocchi, S., Chiaramello, E., Roth, Y., Zangen, A. and Ravazzani, P. (2017) 'Electric field estimation of deep transcranial magnetic stimulation clinically used for the treatment of neuropsychiatric disorders in anatomical head models', *Medical Engineering & Physics*, 43, pp. 30–38. doi: 10.1016/j.medengphy.2017.02.003.

Perera, T., George, M. S., Grammer, G., Janicak, P. G., Pascual-Leone, A. and Wirecki, T. S. (2016) 'The Clinical TMS Society Consensus Review and Treatment Recommendations for TMS Therapy for Major

Depressive Disorder', *Brain Stimulation*. Elsevier Inc., pp. 336–346. doi: 10.1016/j.brs.2016.03.010.

Popa, T., Morris, L. S., Hunt, R., Deng, Z.-D., Horovitz, S., Mente, K., Shitara, H., Baek, K., Hallett, M. and Voon, V. (2019) 'Modulation of Resting Connectivity Between the Mesial Frontal Cortex and Basal Ganglia', *Frontiers in Neurology*. Frontiers, 10, p. 587. doi: 10.3389/fneur.2019.00587.

Pridmore, S., Erger, S., Rybak, M., Kelly, E. and May, T. (2018) 'Early relapse (ER) transcranial magnetic stimulation (TMS) in treatment resistant major depression', *Brain Stimulation*. Elsevier Inc., 11(5), pp. 1098–1102. doi: 10.1016/j.brs.2018.05.013.

Reilly, J. P. and Hirata, A. (2016) 'Low-frequency electrical dosimetry: research agenda of the IEEE International Committee on Electromagnetic Safety', *Physics in Medicine and Biology*. IOP Publishing, 61(12), pp. R138–R149. doi: 10.1088/0031-9155/61/12/R138.

Roth, Y., Zangen, A. and Hallett, M. (2002) 'A coil design for transcranial magnetic stimulation of deep brain regions.', *Journal of clinical neurophysiology : official publication of the American Electroencephalographic Society*, 19(4), pp. 361–70.

Russo, S. J. and Nestler, E. J. (2013) 'The brain reward circuitry in mood disorders', *Nature Reviews Neuroscience*, 14(9), pp. 609–625. doi: 10.1038/nrn3381.

Samoudi, A. M., Tanghe, E., Martens, L. and Joseph, W. (2018) 'Deep Transcranial Magnetic Stimulation: Improved Coil Design and Assessment of the Induced Fields Using MIDA Model', *BioMed Research International*. Hindawi, 2018, pp. 1–9. doi: 10.1155/2018/7061420.

Schlaepfer, T. E., Cohen, M. X., Frick, C., Kosel, M., Brodesser, D., Axmacher, N., Joe, A. Y., Kreft, M., Lenartz, D. and Sturm, V. (2008) 'Deep Brain Stimulation to Reward Circuitry Alleviates Anhedonia in Refractory Major Depression', *Neuropsychopharmacology*, 33(2), pp. 368–377. doi: 10.1038/sj.npp.1301408.

Tendler, A., Barnea Ygael, N., Roth, Y. and Zangen, A. (2016) 'Deep transcranial magnetic stimulation (dTMS) – beyond depression', *Expert Review of Medical Devices*. Taylor and Francis Ltd, pp. 987–1000. doi: 10.1080/17434440.2016.1233812.

Ueno, S., Tashiro, T. and Harada, K. (1988) 'Localized stimulation of neural tissues in the brain by means of a paired configuration of time-varying magnetic fields', *Journal of Applied Physics*. American Institute of Physics, 64(10), pp. 5862–5864. doi: 10.1063/1.342181.

## FIGURES AND TABLES

**TABLE 1**

Electric conductivity values of the head model tissues

| Tissue/bodily fluid | Conductivity [S/m] |
|---|---|
| Amygdala | 0.12 |
| Blood | 0.7 |
| Bone (cancellous) | 0.04 |
| Bone (cortical) | 0.01 |
| Brainstem | 0.07 |
| Caudate | 0.12 |
| Cerebellum gray matter | 0.1 |
| Cerebellum white matter | 0.07 |
| Cerebrospinal fluid | 1.8 |
| Dura | 0.2 |
| Fat | 0.08 |
| Gray matter | 0.12 |
| Hippocampus | 0.12 |
| Intervertebral disc | 0.1 |
| Meninges | 0.2 |
| Mucous membrane | 0.1 |
| Muscle | 0.2 |
| Nucleus accumbens | 0.12 |
| Pallidum | 0.12 |
| Putamen | 0.12 |
| Skin | 0.08 |
| Thalamus | 0.12 |
| Ventral diencephalon | 0.07 |
| Ventricular cerebrospinal fluid | 1.8 |
| Vitreous humor | 1.6 |
| White matter | 0.07 |

**TABLE 2**

Distance from the deep brain regions to the closest point of the scalp

| Deep brain structure | Distance [cm] | Volume [$cm^3$] |
|---|---|---|
| Amygdala | 5.05 ± 0.28 | 2.33 ± 0.06 |
| Brainstem | 6.56 ± 0.33 | 4.39 ± 0.14 |
| Caudate | 4.69 ± 0.22 | 3.00 ± 0.15 |
| Hippocampus | 4.76 ± 0.31 | 3.15 ± 0.16 |
| NAcc | 5.47 ± 0.30 | 1.72 ± 0.10 |
| Putamen | 4.29 ± 0.24 | 3.56 ± 0.20 |
| Thalamus | 5.37 ± 0.26 | 3.94 ± 0.16 |

**TABLE A1**

MSO intensity (%) to generate 50 V/m at deep brain regions ($n$ = 18)

| Region | Circular | Figure-8 | H1 | HFA | HCA | Double Cone | H7 |
|---|---|---|---|---|---|---|---|
| Amygdala | 105.9 | 102.2 | 94.1 | 27.0 | 30.3 | 33.1 | 41.5 |
| Brainstem | 158.8 | 96.6 | 202.9 | 39.4 | 48.9 | 33.1 | 42.1 |
| Caudate | 55.2 | 82.0 | 70.2 | 22.2 | 21.4 | 28.3 | 29.1 |
| Hippocampus | 68.9 | 90.1 | 83.4 | 21.2 | 21.2 | 28.1 | 42.7 |
| NAcc | 115.8 | 94.2 | 130.9 | 36.6 | 37.2 | 32.8 | 38.2 |
| Putamen | 72.2 | 114.7 | 91.4 | 27.7 | 26.5 | 39.2 | 41.2 |
| Thalamus | 83.5 | 146.4 | 142.5 | 35.5 | 32.3 | 48.5 | 72.1 |

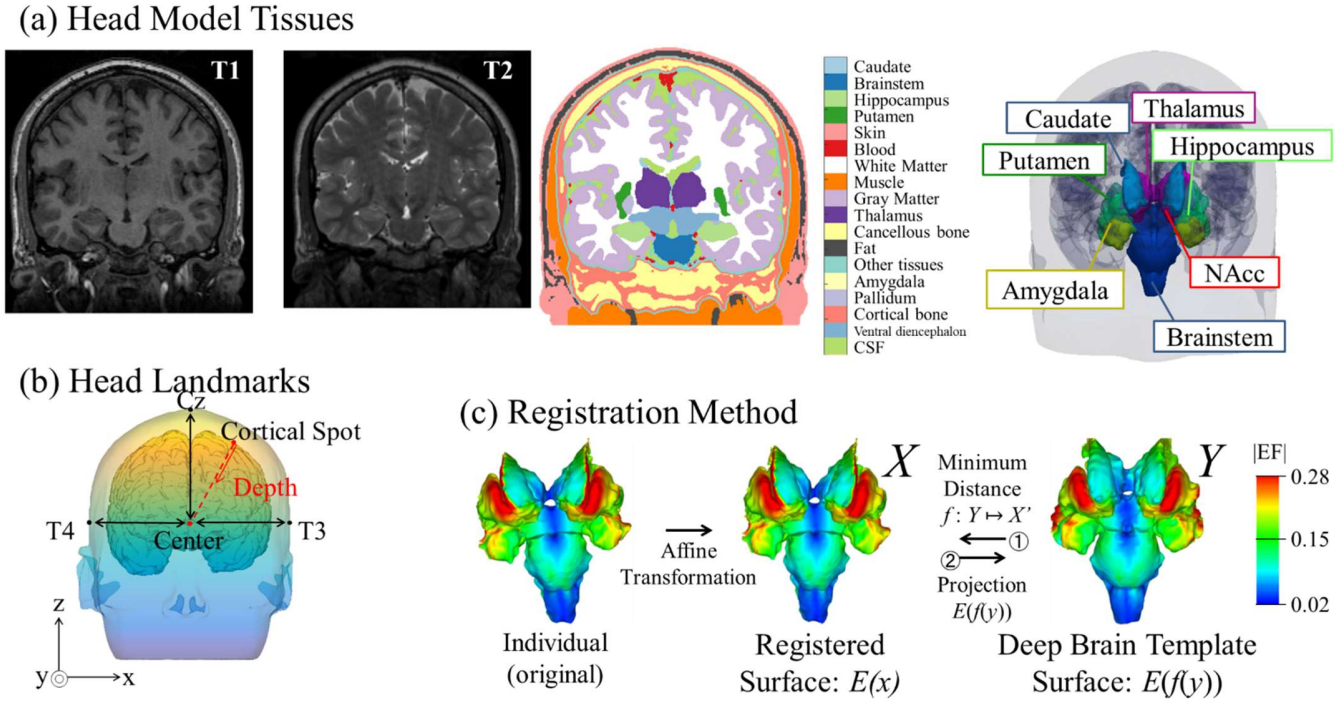


**Figure 1. Segmentation and registration** (a) Head model segmentation including the seven deep brain regions under consideration. (b) Definition of the depth and focality metrics at the "center" of the brain. (c) Registration method of the EFs on the deep-brain-region surfaces to the standard deep-brain template.

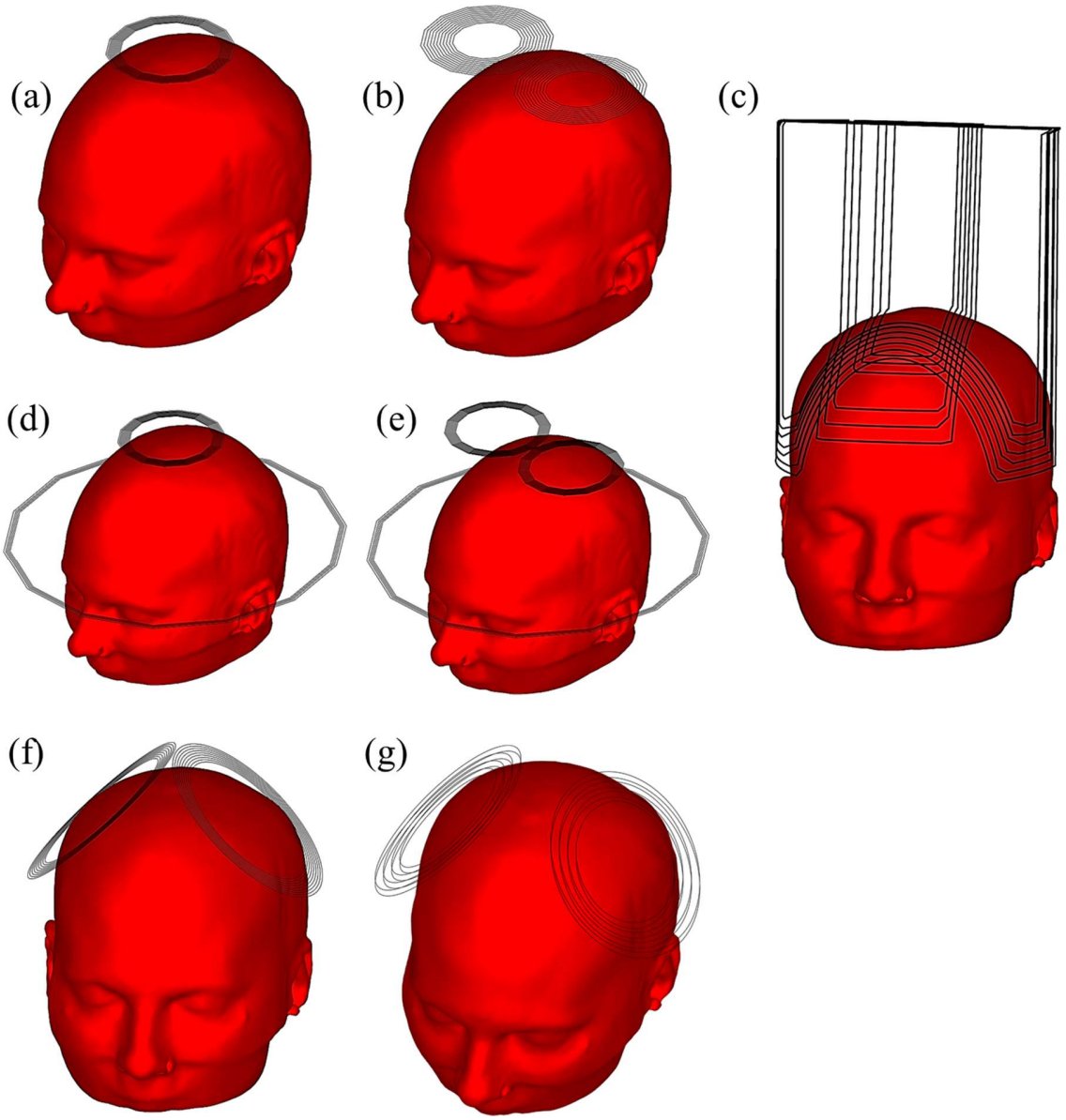


**Figure 2. Comparison of the seven coils**: (a) circular, (b) figure-8, (c) H, (d) HCA, (e) HFA, (f) double cone, and (g) H7 coils for medial-lateral orientation.

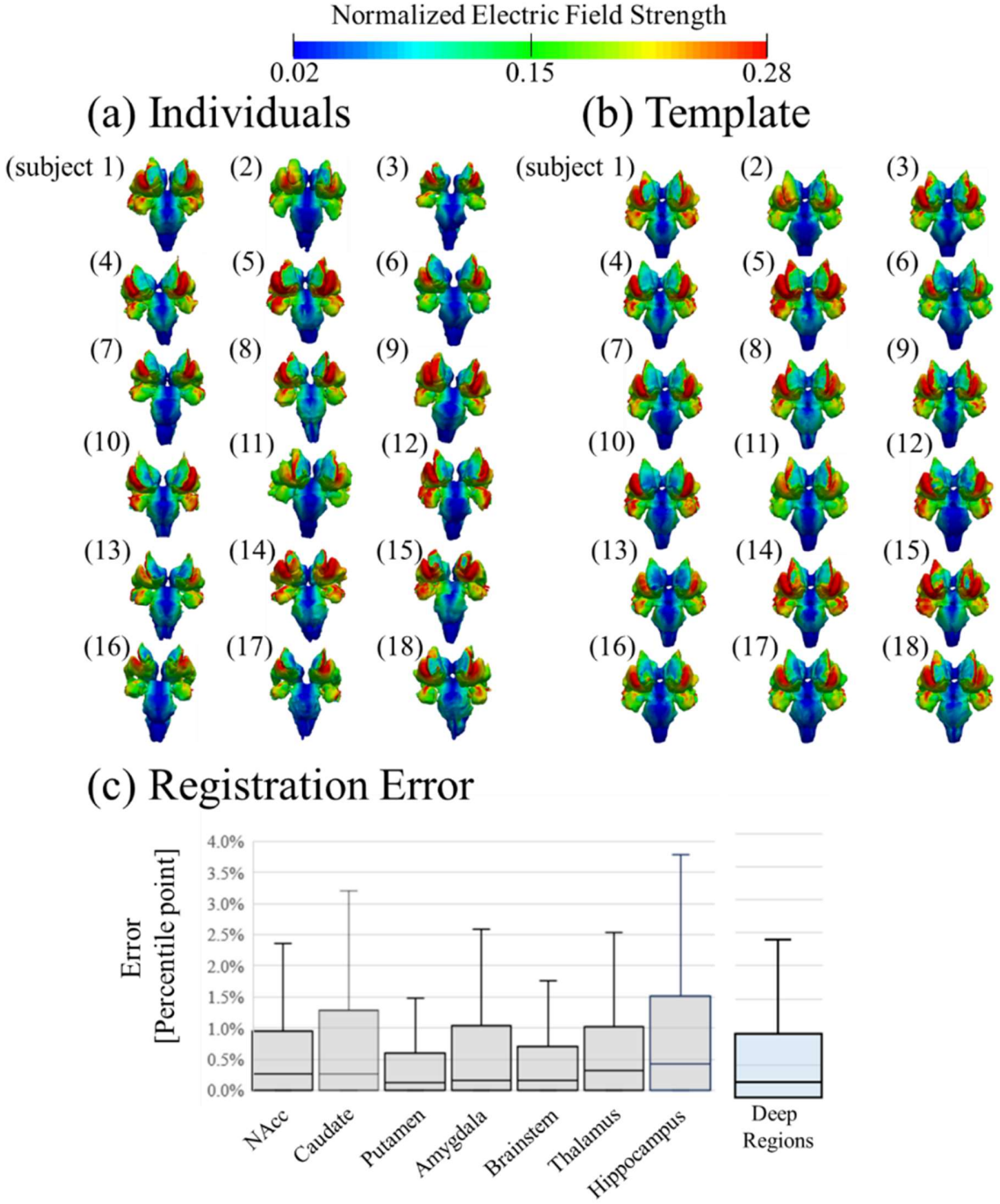


**Figure 3. Individualized EF in the deep brain regions for the HCA** coil centered in Cz position (values are normalized by the maximum cortical EF.). (a) EF distribution of each head model. (b) EF distribution projected on the standard space. (c) Registration error for each deep brain region and whole deep regions for HCA coil ($n$ = 18).

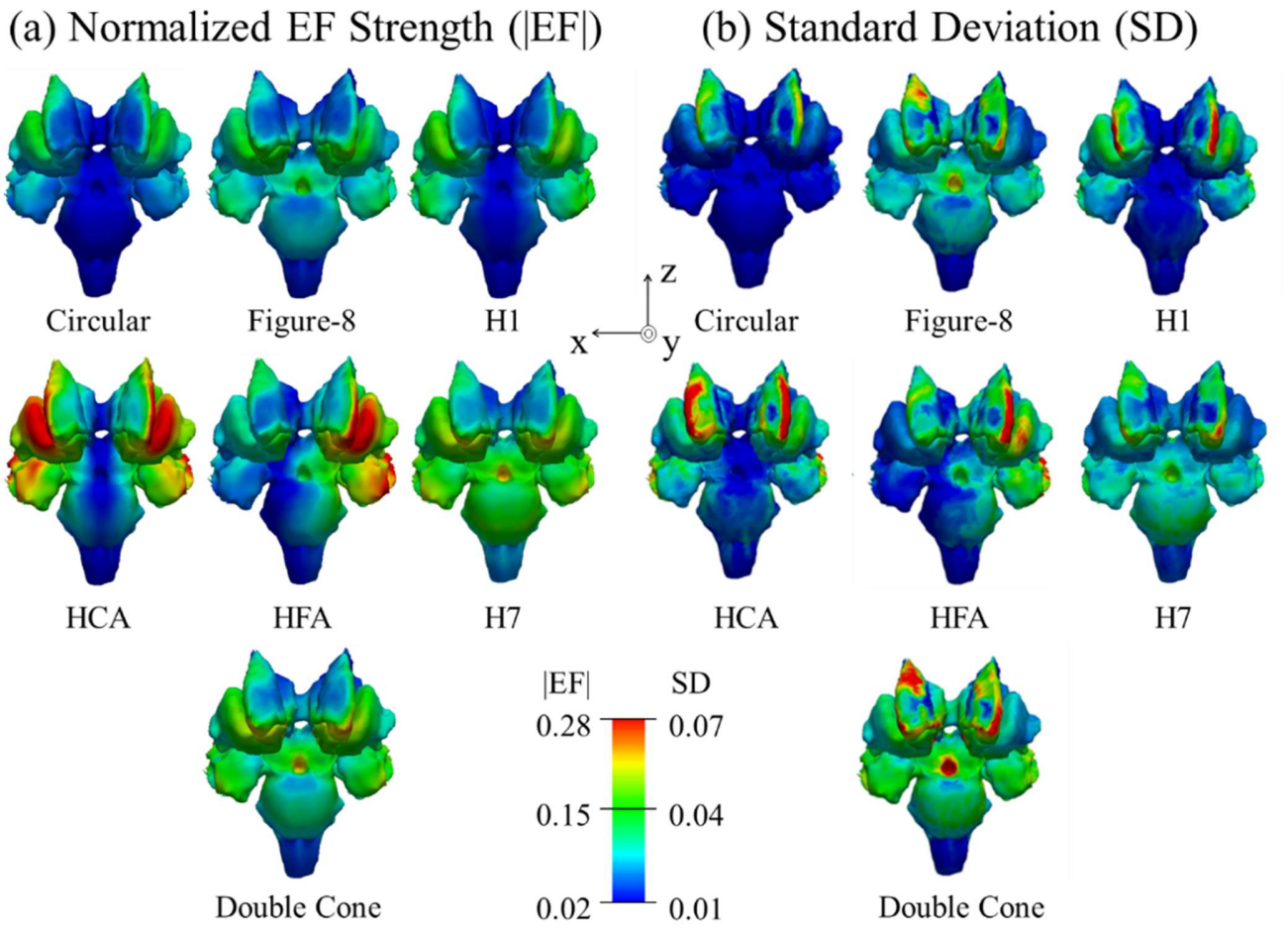


**Figure 4. Group-level EF.** (a) EF averaged over different models ($n$ = 18) in the standard brain space of deep regions for the seven coils centered as Fig. 2. (b) Relative standard deviation of the EF for each coil. Values are normalized by the maximum cortical EF. Note that maximum value is lower than 40%, and an upper limit of 28% was chosen for visualization.

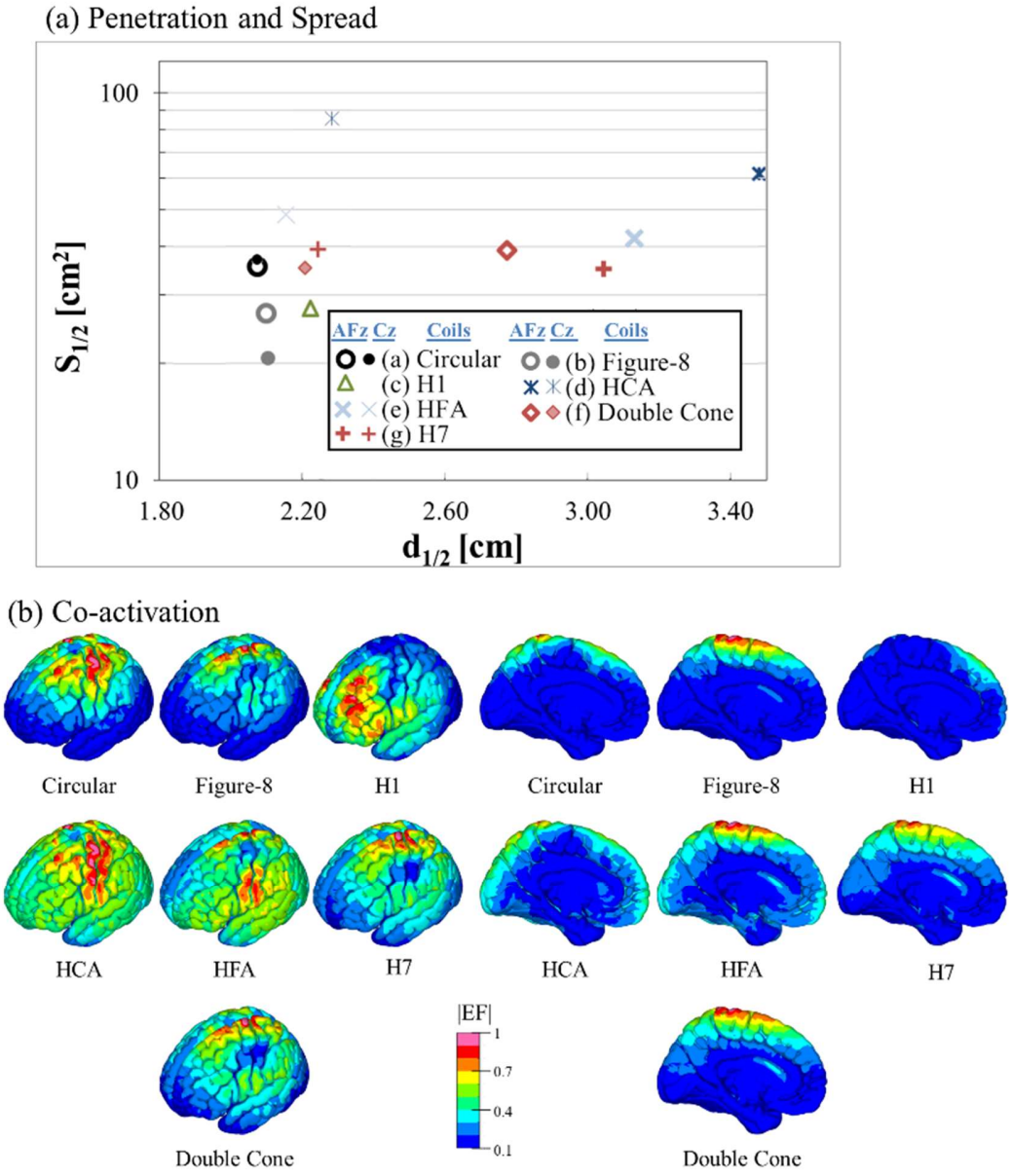


**Figure 5. Coils comparison for a fixed location.** (A) Relationship between spread ($S_{1/2}$) and depth from the cortical surface ($d_{1/2}$) of the EF ($n$ = 18). The coils are placed in two positions, Cz and AFz, according to the EEG system. (B) Group-level EF ($n$ = 18) co-activation in the cerebral cortex and subcortical regions (EFs are normalized by the maximum value) for H1 centered at AFz and the other coils centered at the Cz position.

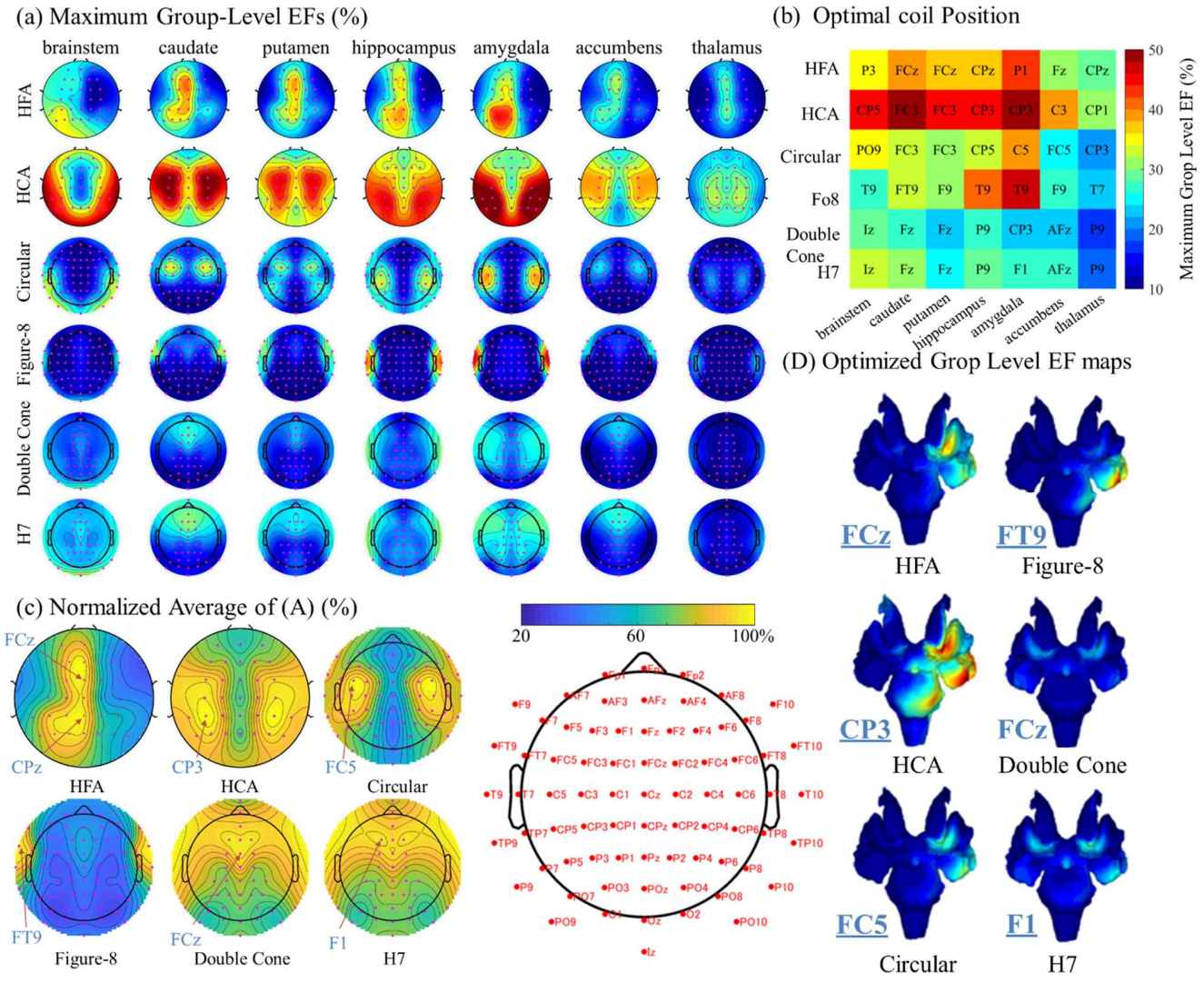


**Figure 6. Optimized Group-level EF.** (A) Scalp EF maps show the maximum group-level EF ($n$ = 18) for individual deep brain regions at different coils positions. (B) The coil position for maximum group-level EF at each deep brain region. (C) Average of the normalized scalp maps for different depth regions. They represent optimized group-level EFs to all deep brain regions. (D) Group-level maps optimized by individual deep regions (panel B) and for all deep brain regions.

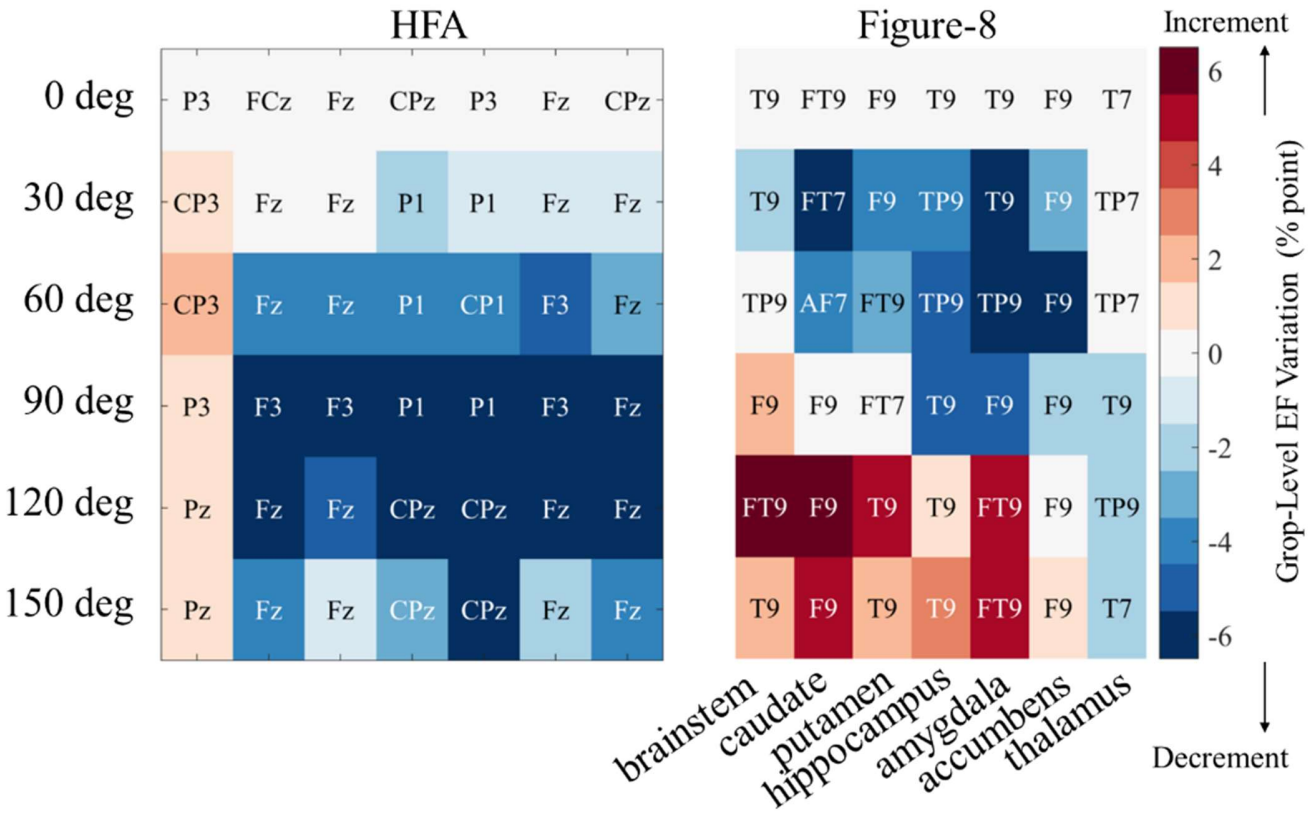


**Figure B1 Coil angle variation effect.** Group-level EF variation at optimized coil positions considering angles from 0° to 150. The percentage point variation with respect to medial–lateral orientation (0°). Optimal coil positions are indicated (10-10 EEG system).